AAS 07-193

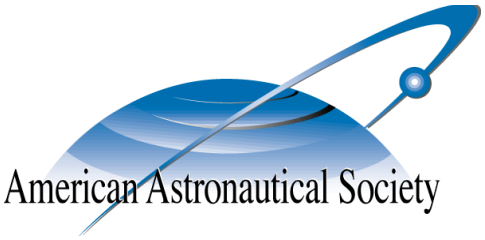

American Institute of
Aeronautics and Astronautics

HYBRID CONTROL OF ORBIT NORMAL AND ALONG-TRACK 2-CRAFT COULOMB TETHERS

Arun Natarajan and Hanspeter Schaub

2007 AAS/AIAA Space Flight Mechanics Meeting

Sedona, Arizona Jan. 28–Feb. 1, 2007

AAS Publications Office, P.O. Box 28130, San Diego, CA 92198

AAS 07-193

HYBRID CONTROL OF ORBIT NORMAL AND ALONG-TRACK 2-CRAFT COULOMB TETHERS

Arun Natarajan* **and Hanspeter Schaub†**

The dynamics and stability of a charged two craft formation with nominal fixed separation distance (Coulomb tethers) is studied where the cluster is aligned with either the along-track or orbit normal direction. Unlike the charged 2-craft formation scenario aligned along the orbit radial direction, a feedback control law using inter-spacecraft electrostatic Coulomb forces and the differential gravitational accelerations is not sufficient to stabilize the Coulomb tether length and the formation attitude. Therefore, a hybrid feedback control law is presented which combines conventional thrusters and Coulomb forces. The Coulomb force feedback requires measurements of separation distance error and error rate, while the thruster feedback is in terms of Euler angles and their rates. This hybrid feedback control is designed to asymptotically stabilize the satellite formation shape and attitude while avoiding plume impingement issues. The effects of differential solar drag on the formation and the ability of the controller to withstand this disturbance is also studied.

INTRODUCTION

Using inter-vehicle electrostatic Coulomb forces for satellite formation flying is a relatively new and emerging concept. Pioneering work in developing this Coulomb formation flying concept is presented in references [1, 2, 3]. Coulomb formation flying works on the principle that by controlling the charge of the spacecraft the inter-craft Coulomb forces can be changed, which in turn can be used to control the relative motion of the spacecraft. With high I_{sp} fuel efficiencies[1, 2] ranging between $10^8 - 10^{13}$ seconds and low Watt-level power requirements, this method of propulsion is considered to be virtually propellantless. The other advantage of this method over conventional thrusters includes clean propulsion without thruster plume contamination issues with neighboring satellites. However, the Coulomb propulsion method also has certain inherent limitations. The Coulomb electrostatic force magnitude is inversely proportional to the square of the separation distance, resulting in the increase of the nonlinear coupling of spacecraft equations of motion. Additionally, the Coulomb force effectiveness is diminished in a space plasma environment due to the presence of charged plasma particles. The electric field strength drops off exponentially with increasing separation distance. The severity of this drop is characterized using the Debye length.[4, 5] For low earth orbits (LEO), the Debye length is of the order of millimeters to centimeters, making the Coulomb formation flying concept impractical at these low orbit altitudes.[6] At high to geostationary orbit (GEO) altitudes the plasma environment is hotter and less dense. As a result the Debye length is much larger and varies between 100-1000 meters depending on the solar activity cycles. Further, the electrostatic charging data of the

*Graduate Student, Aerospace and Ocean Eng. Dep., Virginia Tech, Blacksburg, VA 24061.
†Assistant Professor, Aerospace and Ocean Eng. Dep., Virginia Tech, Blacksburg, VA 24061.

SCATHA spacecraft[7] confirms that spacecraft can charge at least to kilovolt levels in GEO environments, and that the spacecraft charge can be actively controlled through charge emission devices. Thus, Coulomb formation flying concept appears to be feasible at GEO. The currently flying CLUSTER spacecraft also use active charge control.[8] However, the charge emission is applied to zero out the spacecraft potential and not to control relative motion.

References 9 and 10 introduce the concept of a Coulomb tether. Here a conventional mechanical tether cable connecting two crafts is replaced by an electrostatic force which acts as a virtual tether. Conventional tethers are limited to tensile forces whereas Coulomb tethers allow both tensile and compressive forces. However, while traditional spacecraft tether missions consider very large separation distances of multiple kilometers, the Coulomb tether concept is only viable for separation distances up to about 100 meters because of the electrical field strength drop off. Reference 9 studies the stabilization of the simple nadir-aligned static 2-craft Coulomb tether structure. Compared to the previous works on static Coulomb structures,[2,11,12,3] Reference 9 is the first study to introduce a charge feedback law to stabilize a charged spacecraft cluster to a specific shape and orientation. Coulomb forces are inter-spacecraft forces and cannot control the inertial angular momentum of the formation. Hence, stability characteristics of orbital rigid body motion under a differential gravity field is applied to a Coulomb tethered two-spacecraft system to develop an active charge feedback control. With this control the spacecraft separation distance is maintained at a fixed value, while the coupled formation gravity gradient torque is exploited to stabilize the tether attitude about the orbit radial direction. Further, reference 10 investigates the reconfiguring of a nadir-aligned 2-craft Coulomb tether formation by forcing the craft to move apart or come closer using the Coulomb force and again using the gravity gradient to stabilize the formation orientation relative to the orbit radial direction. Gravity gradient rigid satellites or conventional tethers have only bounded stability along the orbit radial direction.[13] Similarly, mechanical tether deployment studies in references 14 and 15 develop length rate laws that guarantee only bounded stability for attitudes. In comparison, the feedback control laws for the Coulomb tether regulation problem in reference 9 and reconfiguration problem in reference 10 guarantee asymptotic stability for separation distance and in-plane angle. This asymptotic stability is achieved by exploiting the charged relative motion of the spacecraft and varying the separation distance (virtual tether length).

Similar to the study of rigid axially symmetric body under the influence of the gravity gradient torque, we know that there are two other relative equilibriums of the charged 2-craft problem other than the orbit radial or nadir direction. These are along the orbit normal and the along-track direction[12] shown in Figure 1. In particular, zero tension is required between the two crafts aligned with the along-track direction to maintain the static unperturbed formation. On the other hand, repulsive forces are required to maintaining the cluster along the orbit normal direction. It is worth noting that both zero tension and compression cases considered are not possible with conventional cable tethers.

This paper studies the stability of a two craft formation about along-track and orbit-normal relative equilibrium configurations. A feedback control law is introduced to asymptotically stabilize both the shape and orientation of this cluster. While the charged 2-craft formation aligned along the orbit radial direction could stabilize the cluster using only Coulomb forces, this study will investigate a hybrid feedback control strategy where both

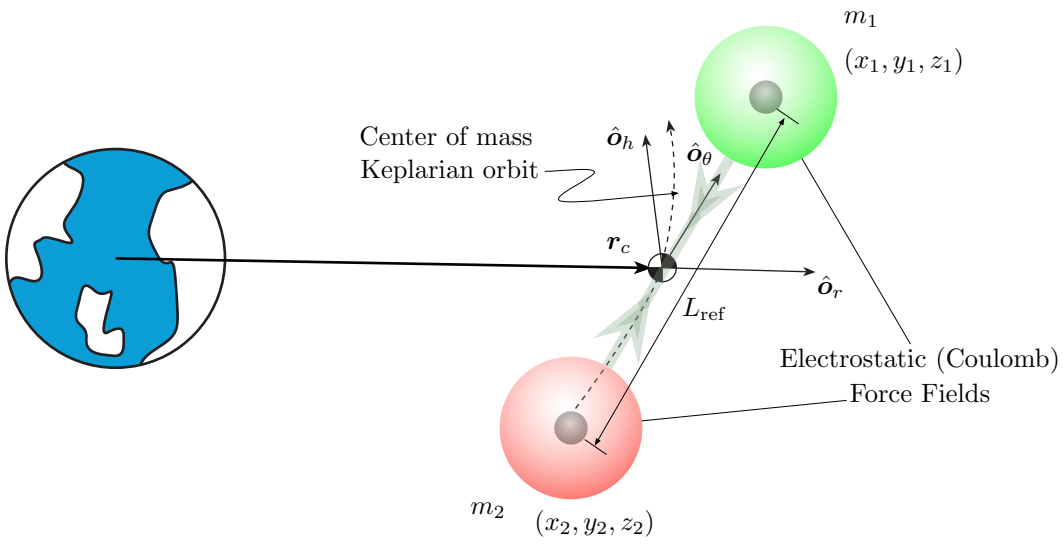

Figure 1 Static Coulomb Tether Formation Aligned with Along-Track Direction.

conventional thrusters and Coulomb forces are used. The goal is to use the thrusters as little as possible and make the Coulomb forces provide the bulk of the actuation requirement. However, to employ small-force thrusters like ion-engines in close proximity to other spacecraft, great care must be taken that the thruster exhaust plume does not impinge on the neighboring craft. These plumes can be very caustic and cause damage to on-board sensors. The control strategy must be designed such that the thruster is never directed at the 2$^{\text{nd}}$ craft.

The formation is studied at GEO where the Debye lengths are large enough to consider Coulomb spacecraft missions. Reference 6 establishes that the differential solar drag is the largest disturbance acting on a Coulomb formation at GEO. Therefor, the effects of differential solar drag on the formation and the ability of the controller to withstand this disturbance is also studied.

CHARGED RELATIVE EQUATIONS OF MOTION

Along-Track Configuration

This section derives the equations of motion of a 2-craft Coulomb tether which is nominally aligned with the along-track direction $\hat{\boldsymbol{o}}_\theta$ of the orbit or Hill frame $\mathcal{O} : \{\hat{\boldsymbol{o}}_r, \hat{\boldsymbol{o}}_\theta, \hat{\boldsymbol{o}}_h, \}$ shown in Figure 1. This derivation closely follows the derivation of the equations of motion for crafts aligned along the orbit radial direction that is given in detail in Reference 9. Figure 1 illustrates a static 2-craft formation in the orbit velocity direction with a separation distance of L_{ref}. Let $Q = q_1 q_2$ be the charge product of the spacecraft charges q_i. The reference charge product Q_{ref} required to maintain this static formation can be computed using the Clohessy-Wiltshire-Hill's equations[13,16,17] for charged spacecraft. The analytical

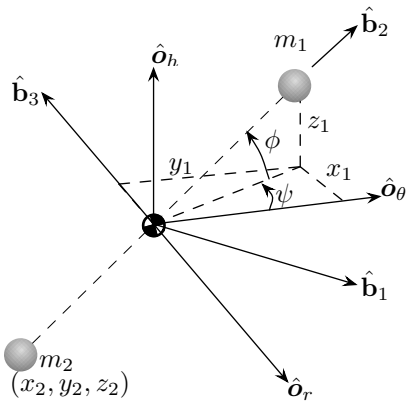

Figure 2 (3-1) Euler Angles Describing the Coulomb Tether Orientation for the Along-Track Relative Equilibria

expression of Q_{ref} for the along-track equilibrium is written as[11]

$$Q_{\text{ref}} = 0 \tag{1}$$

The required relative equilibrium charge is zero because this Coulomb thether configuration is equivalent to a lead-follower spacecraft formation. As a consequence the necessary Coulomb tether tension is zero. However, this static equilibrium is unstable, similar to a rigid rod being unstable if aligned with $\hat{\boldsymbol{o}}_\theta$. The separation distance instability can be stabilized by continuously varying the charges and generating positive or negative tension within the Coulomb tether.

Of interest are the coupled separation distance dynamics and the orientation of the Coulomb tether. Consider the perturbed satellite 1 position (x_1, y_1, z_1) relative to the equilibrium position. The Coulomb tether is only a 1-dimensional structure and thus only requires the $(3-1)$ Euler angles (ψ, ϕ) to define its orientation relative to the orbit frame $\mathcal{O}$. The virtual Coulomb structure body frame $\mathcal{B} : \{\hat{\boldsymbol{b}}_1, \hat{\boldsymbol{b}}_2, \hat{\boldsymbol{b}}_3, \}$ is defined such that $\mathcal{B} = \mathcal{O}$ for zero ψ and ϕ angles, while $\hat{\boldsymbol{b}}_2$ tracks the tether heading. Rotations about $\hat{\boldsymbol{b}}_2$ (θ) can be neglected with point mass assumption of the crafts. The Euler angles are illustrated in Figure 2. Following the same steps as in reference 9, the differential equation of motion for the charged separation distance is given by

$$\ddot{L} = 2\Omega\dot{\psi}L + \frac{k_c}{m_1}Q\frac{1}{L^2}\frac{m_1 + m_2}{m_2} \tag{2}$$

Next the separation distance equations of motion are linearized about small variations in length δL and small variations in the product charge term δQ. The fixed reference separation length L_{ref} is determined by the mission requirement. The reference charge product term for this along-track configuration is known to be zero from Eq. (1).

$$L = L_{\text{ref}} + \delta L \tag{3a}$$

$$Q = Q_{\text{ref}} + \delta Q \tag{3b}$$

Note that these developments treat the required changes in the charge product δQ as the control variable. Substituting these L and Q definitions into Eq. (2) and linearizing leads to

$$\delta\ddot{L} = (2\Omega L_{\text{ref}})\dot{\psi} + \left(\frac{k_c}{m_1}\frac{1}{L_{\text{ref}}^2}\frac{m_1+m_2}{m_2}\right)\delta Q \tag{4}$$

Note that this relationship is coupled to the angular in-orbit-plane rate $\dot{\psi}$. In order to obtain an expression for this, a stability analysis using the gravity gradient is employed. The derivation of the expression for angular perturbation closely follows the derivation given in reference 9 for the orbit radially aligned Coulomb tether. The linearized attitude dynamics of the Coulomb tether body frame are written along with the separation distance equation as:

$$\ddot{\phi} + \Omega^2\phi = 0 \tag{5a}$$

$$\ddot{\psi} + 2\frac{\Omega}{L_{\text{ref}}}\delta\dot{L} - 3\Omega^2\psi = 0 \tag{5b}$$

$$\delta\ddot{L} - (2\Omega L_{\text{ref}})\dot{\psi} - \left(\frac{k_c}{m_1}\frac{1}{L_{\text{ref}}^2}\frac{m_1+m_2}{m_2}\right)\delta Q = 0 \tag{5c}$$

Note that the out-of-plane angle ϕ is decoupled from the separation distance error δL and in-plane angle ψ. Further, the linearized ϕ motion is that of a marginally stable linear oscillator.

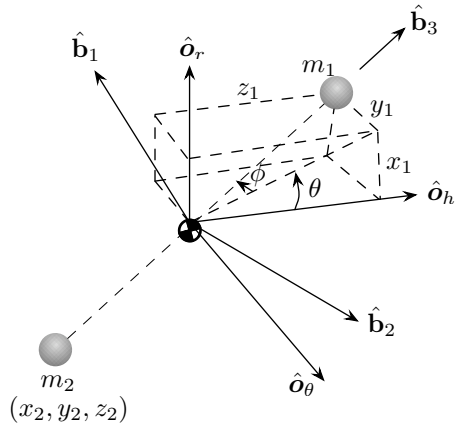

Figure 3 (2-1) Euler Angles Describing the Coulomb Tether Orientation for the Orbit Normal Relative Equilibria

Orbit Normal Configuration

The derivation of the equations of motion for a 2-craft Coulomb tether along orbit normal direction follows the same steps as those of the along-track equilibrium. The analytical expression for the orbit normal relative equilibria charge product Q_{ref} is written as[11]

$$Q_{\text{ref}} = q_1 q_2 = \Omega^2 \frac{L_{\text{ref}}^3}{k_c}\frac{m_1 m_2}{m_1+m_2} \tag{6}$$

Note that $Q_{\text{ref}} > 0$, which requires a repulsive Coulomb force to establish this charged equilibrium. A physical structure in this orientation must compensate for compressive forces, a task conventional tethers are incapable off.

Again, consider small deviations about the equilibrium position and let the $(2-1)$ Euler angles (θ, ϕ) represent the tether body frame $\mathcal{B}$ attitude with respect to the orbit frame $\mathcal{O}$. Here the axis $\hat{\boldsymbol{b}}_3$ tracks the orientation of the orbit-normal tether configuration. The Euler angles are illustrated in Figure 3. Note these angle definitions reflect rotations about the same body axes $\hat{\boldsymbol{b}}_i$ as in the along-track description. However, their zero values are offset by 90 degrees to reflect the different nominal tether orientation.

The differential equation for the separation distance is given by

$$\ddot{L} = -\Omega^2 L + \frac{k_c}{m_1} Q \frac{1}{L^2} \frac{m_1 + m_2}{m_2} \tag{7}$$

We can observe that the separation distance differential equation in Eq. (7) is decoupled from both the orientation angles θ and ϕ. The above equation can be further linearized using Eqs. (3) and the Q_{ref} definition in Eq. (6) to

$$\delta\ddot{L} = -(3\Omega^2)\delta L + \left(\frac{k_c}{m_1} \frac{1}{L_{\text{ref}}^2} \frac{m_1 + m_2}{m_2} \right) \delta Q \tag{8}$$

The differential equation for Euler angles can be obtained similar to the along-track development. The linearized attitude dynamics of the Coulomb tether are written along with the separation distance equation as:

$$\ddot{\phi} - \Omega^2 \phi - 2\Omega\dot{\theta} = 0 \tag{9a}$$

$$\ddot{\theta} - 4\Omega^2 \theta + 2\Omega\dot{\phi} = 0 \tag{9b}$$

$$\delta\ddot{L} + (3\Omega^2)\delta L - \left(\frac{m_1 + m_2}{m_1 m_2} \frac{k_c}{L_{\text{ref}}^2} \right) \delta Q = 0 \tag{9c}$$

Note both the out-of-plane angles θ and ϕ are coupled, while the charged separation distance error dynamics is uncoupled in this linearized formulation. Also, one can observe from Eq. (9c) that the separation distance error (δL) is already marginally stable even with out any feedback control through the charge product error term (δQ).

HYBRID FEEDBACK CONTROL DEVELOPMENT

Along-Track Configuration

In this section, we look into the stability of the linearized along-track equations of motion given Eq. (5) and develop a hybrid feedback control law which stabilizes the system. Reading Eq. (5) it is clear that the out-of-plane angle ϕ is fully decoupled from the in-plane angle ψ and separation distance error δL. The equation of motion for the out-of-plane angle ϕ represents a stable simple harmonic oscillator. Next, consider the coupled in-plane angle ψ and separation distance error δL equations of motion given in Eq. (5b)–(5c). The charge on the craft can be used to control the separation distance since they cause an electrostatic force along the relative position vector. The charge product variation δQ is treated as the

control variable and the feedback control law is defined as

$$\delta Q = \frac{m_1 m_2 L_{\text{ref}}^2}{(m_1+m_2)k_c}(-C_1\delta L - C_2\delta\dot{L}) \tag{10}$$

Here C_1 and C_2 are the position and velocity gains, respectively. Thus, the closed loop equations of motion for the coupled ψ and δL system are written as

$$\ddot{\psi} + 2\frac{\Omega}{L_{\text{ref}}}\delta\dot{L} - 3\Omega^2\psi = 0 \tag{11a}$$

$$\delta\ddot{L} - (2\Omega L_{\text{ref}})\dot{\psi} + C_1\delta L + C_2\delta\dot{L} = 0 \tag{11b}$$

The in-plane angle ψ is coupled with the δL in the form of a driving force ($2\frac{\Omega}{L_{\text{ref}}}\delta\dot{L}$). Hence we select the gains C_1 and C_2 using the Routh-Hurwitz stability criterion to asymptotically stabilize both δL and ψ. The characteristic equation for the equations given in Eq. (11) is

$$\lambda^4 + C_2\lambda^3 + (C_1+\Omega^2)\lambda^2 + (-3C_2\Omega^2)\lambda + (-3C_1\Omega^2) = 0 \tag{12}$$

In order to ensure asymptotic stability, the real parts of the roots of this characteristic polynomial should be negative definite. The constraints on the gains that will guarantee negative definite roots can be identified by constructing a Routh table and are found to be

$$C_2 > 0 \tag{13a}$$

$$C_1 + 4\Omega^2 > 0 \tag{13b}$$

$$\frac{-12C_2\Omega^4}{C_1+4\Omega^2} > 0 \tag{13c}$$

There are no real values for gain C_1 and C_2 that will satisfy all three conditions given in Eq. (13). Hence, the coupled system can not be stabilized with only the Coulomb forces. In addition to the Coulomb forces, we require some thrust forces acting on both satellites along the $\hat{b}_1$ axis that stabilizes the in-plane angle ψ. These thrust forces can be modeled as an equal and opposite force with magnitude F_1. The thrust force magnitude is the second control variable with ψ feedback and it is defined as

$$F_1 = \frac{m_1 m_2}{m_1+m_2}L_{\text{ref}}(K_1\psi) \tag{14}$$

where K_1 is the in-plane angle feedback gain. These forces will introduce a net torque in the ψ equation and the modified coupled equations of motion are written as

$$\ddot{\psi} + 2\frac{\Omega}{L_{\text{ref}}}\delta\dot{L} + (K_1 - 3\Omega^2)\psi = 0 \tag{15a}$$

$$\delta\ddot{L} - (2\Omega L_{\text{ref}})\dot{\psi} + C_1\delta L + C_2\delta\dot{L} = 0 \tag{15b}$$

The characteristic equation for the equations given in Eq. (15) is

$$\lambda^4 + C_2\lambda^3 + (C_1+K_1+\Omega^2)\lambda^2 + (C_2K_1 - 3C_2\Omega^2)\lambda + (C_1K_1 - 3C_1\Omega^2) = 0 \tag{16}$$

The constraints on the gains to ensure asymptotic stability are found using the Routh table to be

$$C_2 > 0 \tag{17a}$$
$$C_1 > -4\Omega^2 \tag{17b}$$
$$K_1 > 3\Omega^2 \tag{17c}$$

The constraints given in Eq. (17) guarantee asymptotic stability, but we need other criteria for fixing their values to yield a satisfactory performance. One way of looking at the problem is to consider the δL equation without the $\dot{\psi}$ term. For ease of discussion, let us rewrite the position and velocity gains in terms of scaling factors n_1 and α_1 as

$$C_1 = n_1\Omega^2 > -4\Omega^2 \tag{18}$$
$$C_2 = \alpha_1\sqrt{n_1}\Omega \tag{19}$$

The δL equation without the $\dot{\psi}$ term is critically damped with $\alpha_1 = 2$. The value of α_1 needs to be altered for achieving near critical damping for the complete δL equation with the $\dot{\psi}$ term. The in-plane angle gain is also rewritten in terms of a scaling factor n_2 as

$$K_1 = n_2\Omega^2 > 3\Omega^2 \tag{20}$$

The natural frequency of the ψ and δL equations are $\sqrt{n_2 - 3}\Omega$ and $\sqrt{n_1}\Omega$, respectively. If n_1 and n_2 are chosen in such a way that these frequencies match, then the $\delta\dot{L}$ term in the ψ equation will act as a defacto damping term and vise versa for the δL equation. The value of n_2 is chosen as 6 as this results in a setting time of about 1 day (1 cycle). For this fixed value of n_2, the root locus for the coupled δL and ψ equations is studied for a range of α_1 values in the vicinity of $\alpha_1 = 2$ with n_1 varying from 0.1 to 20. Based on visual observation of the root locus plots the scaling factors are chosen to be $\alpha_1 = 2.3$ and $n_1 = 2.97$. Figure 4 shows the root locus plot for $n_2 = 6$ and $\alpha_1 = 2.3$, with n_1 varying from 0.1 to 20.

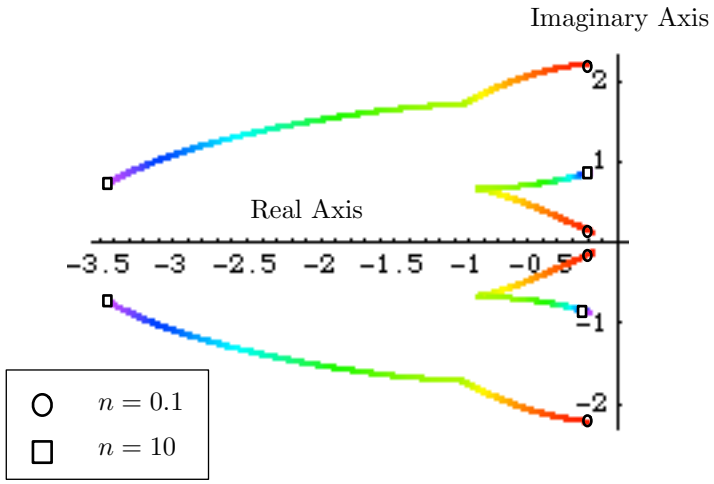

Figure 4 Root Locus Plot for Along-Track Configuration with $n_2 = 6$ and $\alpha_1 = 2.3$.

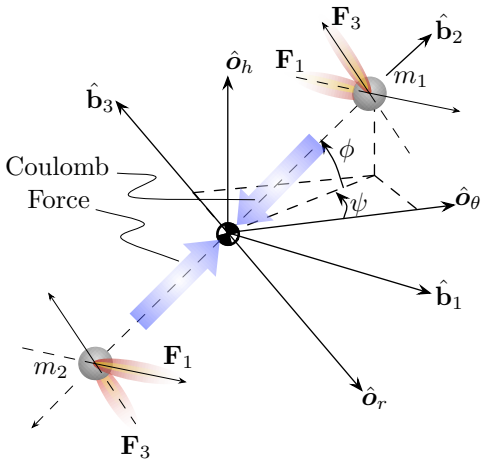

Figure 5 Figure Illustrating the Thrusters Along $\hat{b}_1$ and $\hat{b}_3$ Axes for Along-Track Configuration.

As discussed earlier the equation of motion for the out-of-plane angle ϕ represents a simple harmonic oscillator. This out-of-plane angle can be asymptotically stabilized by using an equal and opposite thrust force on both the satellites along the $\hat{b}_3$ axis. The thrust force magnitude F_3 is the third control variable with $\dot{\phi}$ feedback and it is defined as

$$F_3 = \frac{m_1 m_2}{m_1 + m_2} L_{\text{ref}}(K_2 \dot{\phi}) \tag{21}$$

where K_2 is the out-of-plane angle feedback gain. These forces will introduce a net torque in the ϕ equation and the modified equations of motion are written as

$$\ddot{\phi} + \Omega^2 \phi + K_2 \dot{\phi} = 0 \tag{22}$$

Critical damping is achieved with $K_2 = 2\Omega$. Figure 5 illustrates the thrusters in action along the $\hat{b}_1$ and $\hat{b}_3$ axes for the along-track configuration. For satellite 1, the thrusting force F_1 is acting along the positive $\hat{b}_1$ direction and force F_3 is acting along the negative $\hat{b}_3$ direction. It is vice-versa for satellite 2. Note all thruster forces are directed in orthogonal directions to cluster line of sight vector ($\hat{b}_2$). This avoids any potential plume exhaust impingement issues.

Orbit Normal Configuration

Unlike the along-track configuration, the equation of motion of the separation distance error δL are decoupled from the angles in the orbit normal configuration. The equations of motion of the two out-of-plane angles θ and ϕ are coupled instead. Therefore, the linearized Coulomb forces can be used to stabilized only the separation distance and some thrust force is needed to stabilize the angles. From Eq. (9c), it is clear that without the charge product variation (δQ) term the δL equation of motion about the charged orbit-normal equilibrium represents a stable simple harmonic oscillator. In order to make δL equation of motion asymptotically stable a separation distance error rate ($\delta \dot{L}$) feedback through the control

variable δQ is sufficient. But here we will also introduce a separation distance error (δL) feedback which will enable us to control the natural frequency and thereby the settling time. The feedback control law is given as

$$\delta Q = \frac{m_1 m_2 L_{\text{ref}}^2}{(m_1+m_2)k_c}(-C_1\delta L - C_2\delta\dot{L}) \tag{23}$$

where $C_1 > -3\Omega^2$ and $C_2 > 0$ are the position and velocity feedback gain, respectively. Now, the closed loop separation distance error equation is written as

$$\delta\ddot{L} + (3\Omega^2 + C_1)\delta L + C_2\delta\dot{L} = 0 \tag{24}$$

Fixing $C_2 = 2\sqrt{3\Omega^2 + C_1}$ makes the separation distance equation critically damped.

The coupled out-of-plane angles can be stabilized by using thrust forces on both the satellites. One set of equal and opposite forces with magnitude F_1 act along the $\hat{b}_1$ axis. The other set of forces with magnitude F_2 act along the $\hat{b}_2$ axis. The feedback control law for the thrust force magnitudes are defined as

$$F_1 = \frac{m_1 m_2}{m_1+m_2} L_{\text{ref}}(K_2\theta) \tag{25}$$

$$F_2 = \frac{m_1 m_2}{m_1+m_2} L_{\text{ref}}(K_1\phi + K_3\dot{\phi}) \tag{26}$$

where K_1 and K_3 are the angle and angle rate gains for ϕ, and K_2 is the angle gain for θ. It should be noted that the thrust forces F_1 and F_2 stabilize the out-of-plane angles θ and ϕ, respectively. Further, these forces too only act orthogonal to the line of sight vector of the 2 craft, thus avoiding plume impingement issues. These forces introduce torque into the angular equations of motion and the augmented coupled closed loop equations are

$$\ddot{\phi} - 2\Omega\dot{\theta} + (K_1 - \Omega^2)\phi + K_3\dot{\phi} = 0 \tag{27a}$$

$$\ddot{\theta} + (K_2 - 4\Omega^2)\theta + 2\Omega\dot{\phi} = 0 \tag{27b}$$

The characteristic equation of the coupled equations of motion given in Eq. (27) is

$$\lambda^4 + K_3\lambda^3 + (K_1 + K_2 - \Omega^2)\lambda^2 + (K_2K_3 - 4K_3\Omega^2)\lambda + (K_1K_2 - 4K_1\Omega^2 - K_2\Omega^2 + 4\Omega^2) = 0 \tag{28}$$

The characteristic equation with roots having negative real parts will guarantee asymptotic stability. The constraints on the gains that will result in the characteristic equation given in Eq. (28) to have negative define roots, can be established with Routh-Hurwitz criterion. The constraints on the gains are

$$K_1 > \Omega^2 \tag{29a}$$

$$K_2 > 4\Omega^2 \tag{29b}$$

$$K_3 > 0 \tag{29c}$$

Before we proceed to establish the value of the gains, it is important to note that with out the $\dot{\phi}$ feedback the characteristic equation would have been

$$\lambda^4 + (K_1 + K_2 - 2\Omega^2)\lambda^2 + (K_1K_2 - 4K_1\Omega^2 - K_2\Omega^2 + 4\Omega^2) = 0 \tag{30}$$

and one can come up with gains that will only guarantee marginal stability, but not convergence. This justifies the use of angle rate ($\dot{\phi}$) feedback for achieving asymptotic stability.

The gains values are fixed in such a way that they guarantee near critical damping. The gains K_1 and K_3 are rewritten in terms of scaling factors n and α as

$$K_1 = n\Omega^2 > \Omega^2 \tag{31}$$
$$K_3 = \alpha\sqrt{(n-1)}\Omega \tag{32}$$

In the ϕ equation of motion, $\alpha = 2$ guarantees critical damping if one ignores the $\dot{\theta}$ term. For fixed values of $K_2 > 4\Omega^2$, the root locus for the coupled θ and ϕ equations is studied for a range of α values in the vicinity of $\alpha = 2$ with n varying from 1.1 to 10. Based on visual observation of the root locus plots the gain K_2 is chosen to be $5\Omega^2$ and the scaling factors are chosen to be $\alpha = 2.5$ and $n = 2.7$. Figure. 6 shows the root locus plot for $K_2 = 5\Omega^2$ and $\alpha = 2.5$, with n varying from 1.1 to 10.

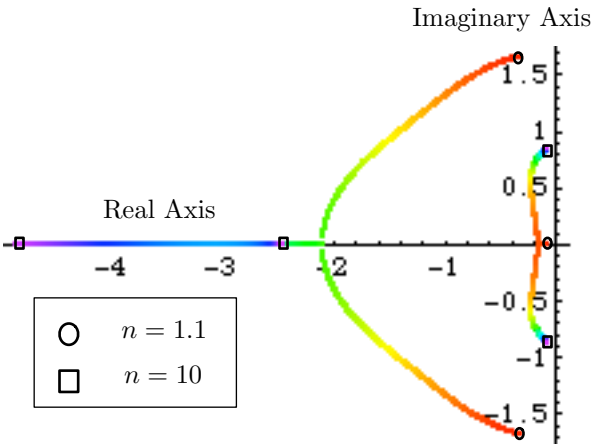

Figure 6 Root Locus Plot for Orbit Normal Configuration with $K_2 = 5\Omega^2$ and $\alpha = 2.5$

NUMERICAL SIMULATION

This section presents numerical simulations of the along-track and orbit normal Coulomb tether formations to illustrate the performance and stability of the presented hybrid feedback control strategy. The Coulomb tether performance is simulated in two different manners. First the linearized spherical coordinate differential equations are integrated. This simulation illustrates the linear performance of the charge control. Second, the linearized results are compared with those obtained from the exact nonlinear equation of motion of the deputy satellites given by

$$\ddot{\boldsymbol{r}}_1 + \frac{\mu}{r_1^3}\boldsymbol{r}_1 = \frac{k_c}{m_1}\frac{Q}{L^3}(\boldsymbol{r}_1 - \boldsymbol{r}_2) \tag{33a}$$
$$\ddot{\boldsymbol{r}}_2 + \frac{\mu}{r_2^3}\boldsymbol{r}_2 = \frac{k_c}{m_2}\frac{Q}{L^3}(\boldsymbol{r}_2 - \boldsymbol{r}_1) \tag{33b}$$

where $\boldsymbol{r}_1 = \boldsymbol{r}_c + \boldsymbol{\rho}_1$ and $\boldsymbol{r}_2 = \boldsymbol{r}_c + \boldsymbol{\rho}_2$ are the inertial position vectors of the the masses m_1 and m_2, while $L = \sqrt{(\boldsymbol{r}_2 - \boldsymbol{r}_1) \cdot (\boldsymbol{r}_2 - \boldsymbol{r}_1)}$. The gravitational coefficient μ is defined as $\mu \approx GM_e$. After integrating the motion using inertial Cartesian coordinates, the separation distance L, as well as the corresponding angles are computed in post-processing using the exact kinematic transformation. Finally, the robustness of the control laws is illustrated in the presence of differential solar perturbation. For all cases the cluster center of mass is assumed to be a GEO orbit.

Along-Track Configuration

The along-track Coulomb tether with a separation distance of 25 meter is simulated first. The input parameters are given in Table 1. The initial separation distance error (δL) is set to 0.5 meter and the Euler angles are set to $\psi = 0.1$ radians and $\phi = 0.1$ radians. All initial rates are set to zero through $\dot{\psi} = \delta\dot{L} = \dot{\phi} = 0$. As discussed in the previous section, the gain values are chosen based on studying the root locus plot to be $C_1 = 2.97\Omega^2$, $C_2 = 3.9637\Omega$, $K_1 = 6\Omega^2$ and $K_2 = 2\Omega$.

Table 1 Input Parameters Used in Along-Track Simulation

Parameter	Value	Units
m_1	150	kg
m_2	150	kg
L_{ref}	25	m
k_c	8.99×10^9	$\frac{\text{Nm}^2}{\text{C}^2}$
Q_{ref}	0	μC^2
Ω	7.2915×10^{-5}	rad/sec
C_1	$2.97\Omega^2$	
C_2	3.9637Ω	
K_1	$6\Omega^2$	
K_2	2Ω	
$\delta L(0)$	0.5	m
$\psi(0)$	0.1	rad
$\phi(0)$	0.1	rad

Figure 7(a) shows the Coulomb tether motion in both linearized spherical coordinates δL, ψ and ϕ (continuous line), and the full nonlinear spherical coordinates (dashed lines). It shows that the nonlinear simulation closely follows the linear simulation, validating the linearizing assumptions. The charge feedback law augmented with the thrust forces (using angle and angle rate feedback) ensures the convergence of all states to zero. Figure 7(b) illustrates the control charge on a single spacecraft for both linearized and full nonlinear simulation models. The reference charge pertaining to static equilibrium for along-track formation is zero and control charges are converging to this value. Note that the deviation from the value of reference charges is small, justifying the charge linearization assumptions used. The magnitude of the control charges is in the order of micro-Coulomb which is easily

realizable in practice using charge emission devices. Figure 7(c) gives the thrusting force that is required to stabilize the angles. Again, the dashed lines represent the full nonlinear model and the continuous lines represent the linearized model. The thrust forces can be generated using conventional thrusters. In the body fixed coordinates, the crafts are aligned along the $\hat{b}_2$ axis and the thrust forces F_1 and F_2 are acting along the $\hat{b}_1$ and $\hat{b}_3$ directions, respectively. Thus, the thrusting always takes place at an axis that is perpendicular the craft orientation, thereby avoiding plume impingement issues.

Orbit Normal Configuration

The orbit normal Coulomb tether is also simulated with a separation distance of 25 meter like the along-track configuration. The same spacecraft parameters and nominal separation distance are used as in Table 1. The initial separation distance error, initial Euler angles and gains are given in Table 2. Figures 8(a) , 8(b), 8(c) show the tether motion (spherical coordinates), charge on a single craft and thrust forces, respectively. Again, the dashed lines depicting the full nonlinear model closely follow continuous lines depicting the linearized model. It can be observed from Figure 8(a) that the separation distance error is critically damped and the out-of-plane angles ϕ and θ asymptotically go to zero. The thrust forces F_1 and F_2 are acting in the $\hat{b}_1$ and $\hat{b}_2$ direction with the Coulomb tether aligned along the $\hat{b}_3$ direction. Thus, plume impingement problems are avoided.

Table 2 Input Parameters Used in Orbit Normal Simulation

Parameter	Value	Units
Q_{ref}	6.9304×10^{-13}	μC^2
C_2	$2\sqrt{3}\Omega$	
K_1	$2.7\Omega^2$	
K_3	3.2596Ω	
K_2	$5\Omega^2$	
$\delta L(0)$	0.5	m
$\theta(0)$	0.06	rad
$\phi(0)$	0.04	rad

Differential Solar Perturbation

At GEO, differential solar drag is the largest disturbance acting on the Coulomb formation. Hence, full nonlinear model simulation for both along-track and orbit normal configuration are carried out including the effects of solar drag to study the ability of the controller to withstand this disturbance. The inertial acceleration vector $\mathbf{r_s}$ due to the effects of solar radiation pressure is given as

$$\mathbf{r_s} = \frac{-C_r A F}{mc} \frac{\mathbf{r}}{||\mathbf{r}||^3} \tag{34}$$

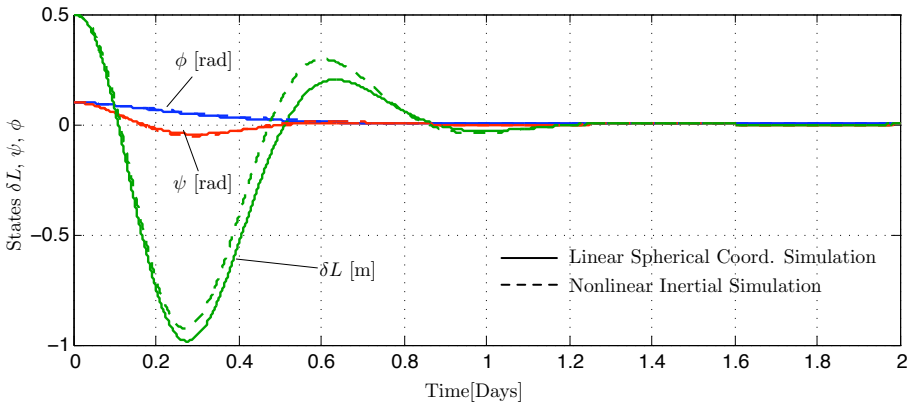

(a) Time histories of length variations δL, in-plane rotation angle ψ, and out-of-plane rotation angle ϕ.

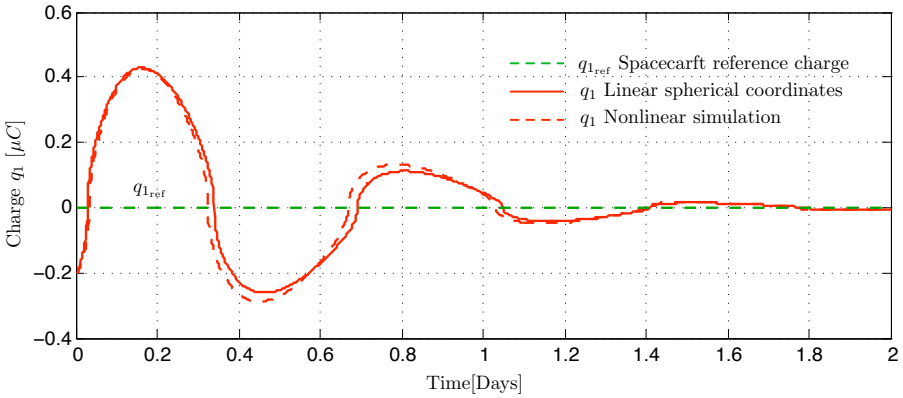

(b) Spacecraft charge time histories

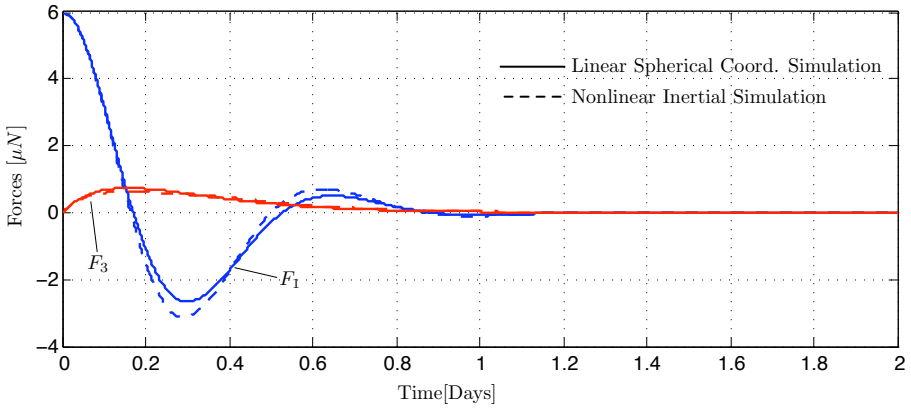

(c) Spacecraft force time histories

Figure 7 Simulation results for two crafts aligned along the along-track direction with a separation distance of 25m.

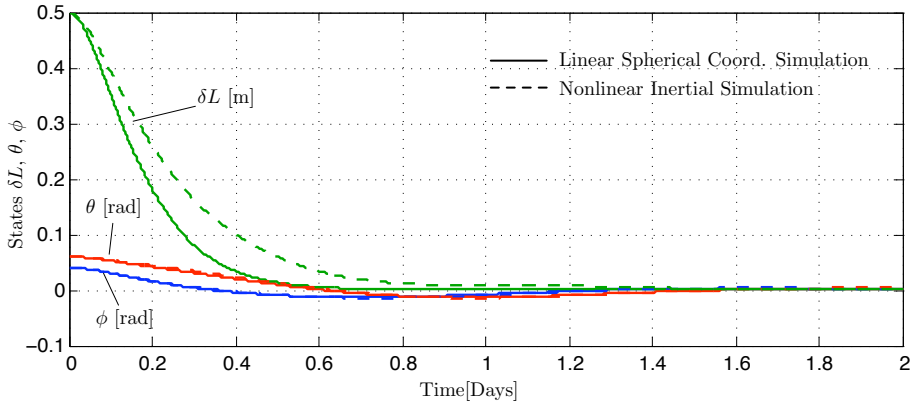

(a) Time histories of length variations δL, out-of-plane rotation angles θ and ϕ.

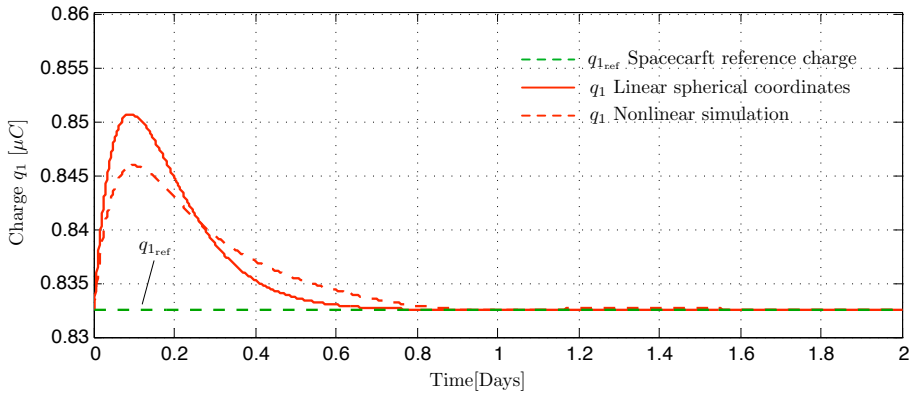

(b) Spacecraft charge time histories

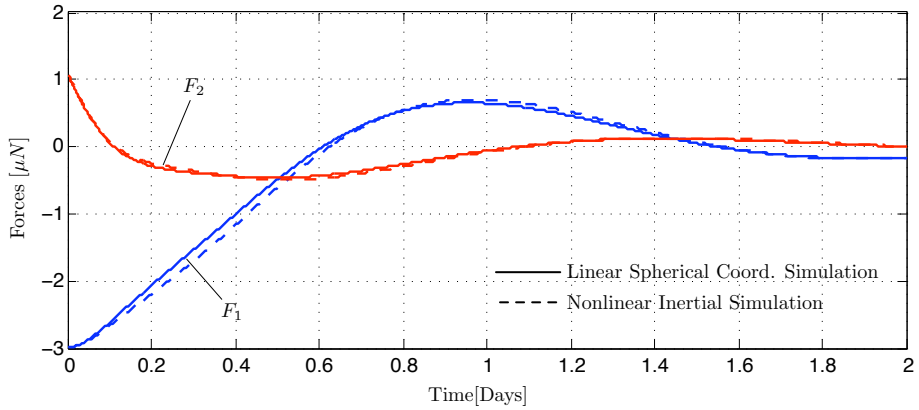

(c) Spacecraft force time histories

Figure 8 Simulation results for two crafts aligned along the orbit normal direction with a separation distance of 25m.

where $\mathbf{r}$ is the position vector from the sun to the orbiting planet in AU, m is the mass of the spacecraft in kg, A is the cross section area of the spacecraft that is facing the sun in m^2. The constant $F = 1372.5398$ Watts/m^2 is the solar radiation flux, $c = 2.997 \times 10^8$ m/s is the speed of light, and $C_r = 1.3$ is the radiation pressure coefficient.

The simulation is carried out over a period of 3 days and the Sun's position is assumed to be fixed with respect to the Earth fixed inertial coordinates. As shown in Figure 9, the solar rays are assumed to be making an angle of $23^o27^{'}$ with respect to the earth's equatorial plane to account for the earth's axial tilt. The craft are modeled as cylinders with radius of 0.5 m, height of 1 m and mass of 150 kg. For craft 1, the cylindrical surface is constantly facing the sun resulting in a square cross section area of 1 m^2, where as for craft 2, it is the circular cross section (0.25π m^2)of the top of the cylinder that is facing the sun.

Figure 10(a) shows the time histories of the spherical coordinates δL, ψ and ϕ for along-track Coulomb tether formation with differential solar drag. The coupled states δL and ψ no longer asymptotically converge to zero, but they are still bounded. The in-plane angle ψ oscillates with maximum amplitude of ± 0.05 radians and the separation distance error δL oscillations are negligible. The out-of-plane motion ϕ settles with a constant steady state offset. This offset can be explained by looking at the linearized ϕ equation of motion. The ϕ equation is decoupled and with a constant external torque due to the differential solar drag, will result in a steady state offset. Let the constant inertial acceleration vector along the $\hat{o}_h$ direction due to solar drag for satellites one and two be $\mathbf{r_{s1}}(3,1)$ and $\mathbf{r_{s2}}(3,1)$, respectively. The total constant force acting on the satellite formation along the $\hat{o}_h$ direction is

$$F_s = m_1 \mathbf{r_{s1}}(3,1) + m_2 \mathbf{r_{s2}}(3,1)$$

The resulting torque due to this force is given by

$$T_s = \frac{m_1}{m_1 + m_2} L(m_1 \mathbf{r_{s1}}(3,1)) - \frac{m_2}{m_1 + m_2} L(m_2 \mathbf{r_{s2}}(3,1)) \tag{35}$$

The linearized ϕ equation for along track configuration (Eq. (5a)) can be modified to incorporate the constant torque given in Eq. (35) as

$$\ddot{\phi} + \Omega^2 \phi = \frac{\frac{1}{m_1+m_2} L(m_1^2 \mathbf{r_{s1}}(3,1) - m_2^2 \mathbf{r_{s2}}(3,1))}{\frac{m_1 m_2}{m_1+m_2} L^2} \tag{36}$$

From Eq. (36), the analytical expression for steady state offset in the presence of differential solar drag can be written as

$$\phi = \frac{(m_1/m_2 \mathbf{r_{s1}}(3,1) - m_2/m_1 \mathbf{r_{s2}}(3,1))}{L\Omega^2} \tag{37}$$

For the linearized model the offset was calculated to be -0.0255 radians and it is very close to the offset observed for the full nonlinear model. Figures 10(b) and 10(c) give the spacecraft charge and thrust force time histories, respectively.

Figure 11(a) shows the performance of orbit normal Coulomb tether in the presence of differential solar drag. Again, it can be observed that the states are bounded. On close observation of the figure one can come to the conclusion that the separation distance error (δL) is oscillating about an offset at steady state. The linearized separation distance error

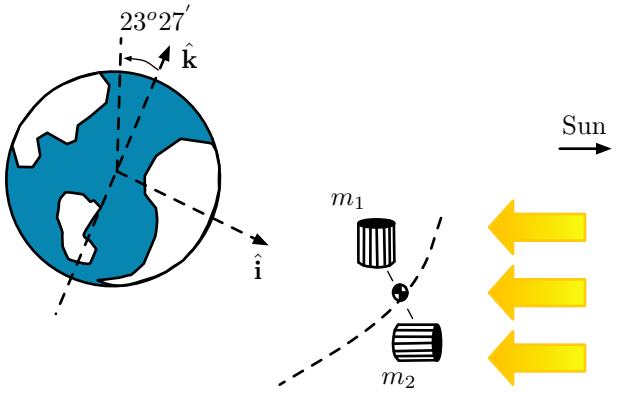

Figure 9 Figure Illustrating the Orientation of the Cylindrical Craft and the Sun's Position

(δL) is decopled from the angles and constant differential solar drag acting on the formation results in a steady state offset for δL. The analytical expression for this steady state δL offset can be derived for the linearized model as

$$\delta L = \frac{(m_1 \mathbf{r_{s1}}(3,1) - m_2 \mathbf{r_{s2}}(3,1))}{3m_1\Omega^2} \tag{38}$$

Thus, the linearized model offset for δL is -0.2125 m. The observed steady state offset in the figure is close to this value and the oscillations can be explained due to the second order coupling of the separation distance error (δL) with the angles. The oscillations in the δL result in the oscillations of the spacecraft charge value around the reference charge value, as seen in Figures 11(b). Figures 11(c) shows the thrust force time histories.

CONCLUSION

A 2-craft Coulomb tethered structure aligned along the orbit normal or along-track direction cannot be stabilized with only a charge feedback law. But, both Coulomb tether configurations can be stabilized with a hybrid control of Coulomb forces and conventional thrusters that stabilize the separation distance and orientation respectively. The control charges needed are small in the order of micro-Coulombs and realizable in practice. The thrusting forces required are in the order of micro-Newtons and the thrusting is always done orthogonal to the Coulomb tether axis, thus avoiding plume exhaust impingement problems. For the along-track configuration the separation distance and in-plan angle are coupled and unstable without feedback. An interesting result is that for the orbit-normal configuration the separation distance is decoupled and marginally stable even without charge feedback, while the orientation has to be feedback stabilized. Numerical simulations of the full nonlinear motion are carried out to illustrate the results and compare the linearized performance predictions to the actual nonlinear system response. Finally, the robustness of the controller to withstand differential solar drag is illustrated through simulations.

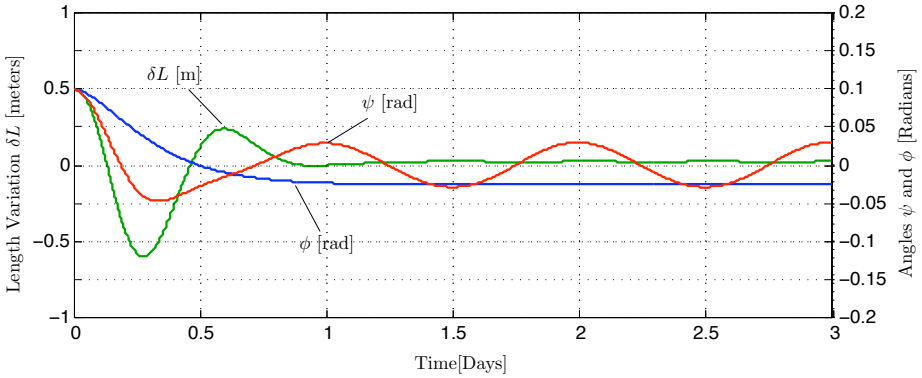

(a) Time histories of length variations δL, out-of-plane rotation angles θ and ϕ.

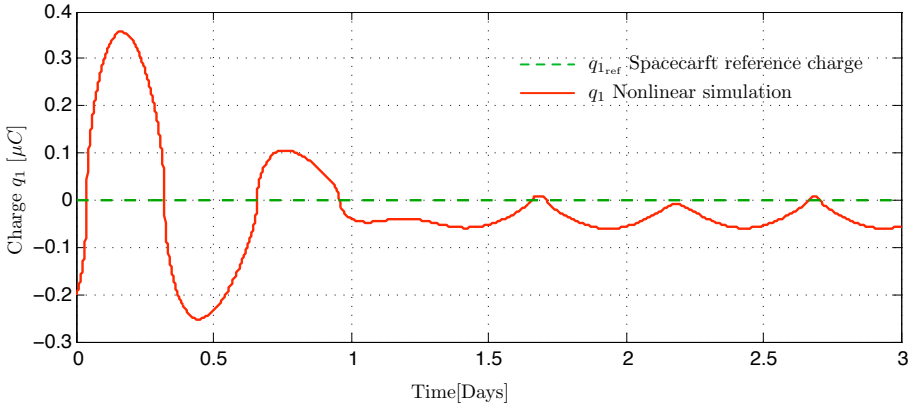

(b) Spacecraft charge time histories

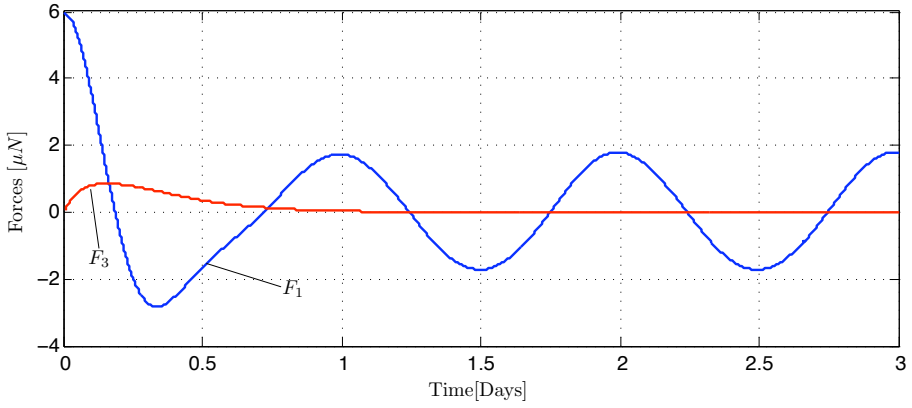

(c) Spacecraft force time histories

Figure 10 Simulation results for two crafts aligned along the along-track direction with constant differential solar perturbation.

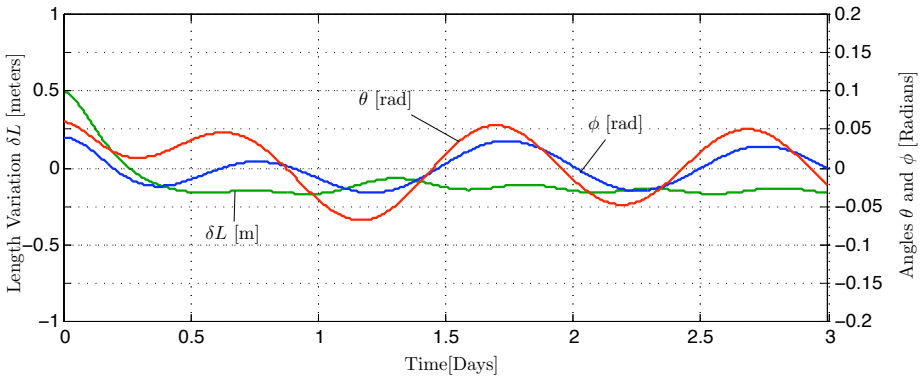

(a) Time histories of length variations δL, out-of-plane rotation angles θ and ϕ.

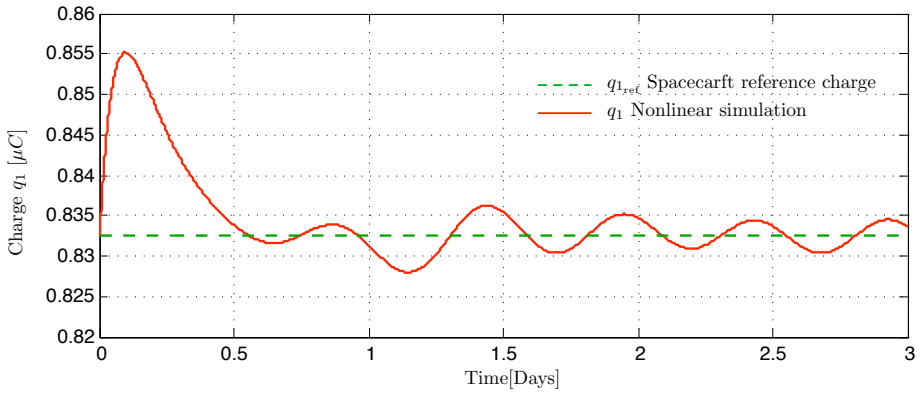

(b) Spacecraft charge time histories

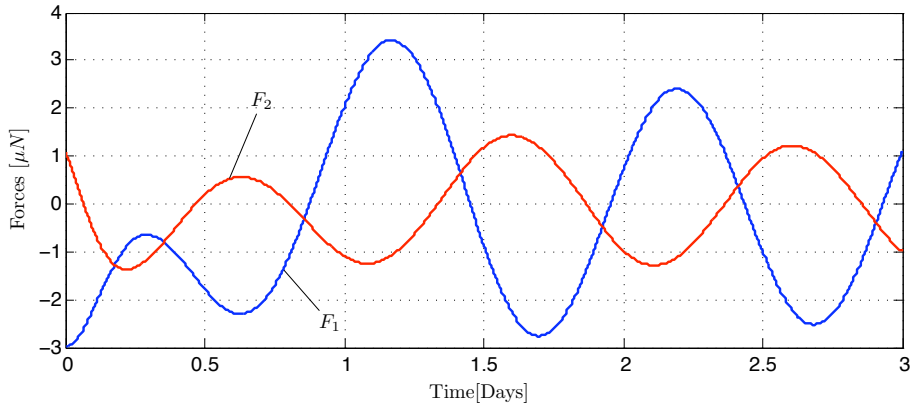

(c) Spacecraft force time histories

Figure 11 Simulation results for two crafts aligned along the orbit normal direction with constant differential solar perturbation.

REFERENCES

[1] L. B. King, G. G. Parker, S. Deshmukh, and J.-H. Chong, "Spacecraft Formation-Flying using Inter-Vehicle Coulomb Forces," tech. rep., NASA/NIAC, January 2002. `http://www.niac.usra.edu`.

[2] L. B. King, G. G. Parker, S. Deshmukh, and J.-H. Chong, "Study of Interspacecraft Coulomb Forces and Implications for Formation Flying," *AIAA Journal of Propulsion and Power*, Vol. 19, May–June 2003, pp. 497–505.

[3] H. Schaub, G. G. Parker, and L. B. King, "Challenges and Prospect of Coulomb Formations," *AAS John L. Junkins Astrodynamics Symposium*, College Station, TX, May 23-24 2003. Paper No. AAS-03-278.

[4] D. R. Nicholson, *Introduction to Plasma Theory*. Krieger, 1992.

[5] T. I. Gombosi, *Physics of the Space Environment*. Cambridge University Press, 1998.

[6] C. C. Romanelli, A. Natarajan, H. Schaub, G. G. Parker, and L. B. King, "Coulomb Spacecraft Voltage Study Due to Differential Orbital Perturbations," *AAS/AIAA Space Flight Mechanics Meeting*, Tampa, Florida, Jan. 2006. Paper No. AAS 06-123.

[7] E. G. Mullen, M. S. Gussenhoven, D. A. Hardy, T. A. Aggson, B. G. Ledley, and E. Whipple, "SCATHA Survey of High-Level Spacecraft Charging in Sunlight," *Journal of the Geophysical Sciences*, Vol. 91, Feb. 1986, pp. 1474–1490.

[8] K. Torkar and et. al., "Active Spacecraft Potential Control for Cluster – Implementation and First Results," *Annales Geophysicae*, Vol. 19, 2001, pp. 1289–1302.

[9] A. Natarajan and H. Schaub, "Linear Dynamics and Stability Analysis of a Two-Craft Coulomb Tether Formation," *AIAA Journal of Guidance, Control, and Dynamics*, Vol. 29, Jul.–Aug. 2006, pp. 831–839.

[10] A. Natarajan and H. Schaub, "Reconfiguration of a 2-Craft Coulomb Tether," *AAS/AIAA Space Flight Mechanics Meeting*, Tampa, Florida, Jan. 2006. Paper No. AAS 06-229.

[11] J. Berryman and H. Schaub, "Analytical Charge Analysis for 2- and 3-Craft Coulomb Formations," *AAS/AIAA Astrodynamics Specialist Conference*, Lake Tahoe, Aug. 2005. Paper No. 05-278.

[12] J. Berryman and H. Schaub, "Static Equilibrium Configurations in GEO Coulomb Spacecraft Formations," *AAS/AIAA Space Flight Mechanics Meeting*, Copper Mountain, Colorado, Jan. 2005. Paper No. AAS 05-104.

[13] H. Schaub and J. L. Junkins, *Analytical Mechanics of Space Systems*. Reston, VA: AIAA Education Series, October 2003.

[14] D. M. Xu, A. K. Misra, and V. J. Modi, "Three-Dimensional Control of the Shuttle Supported Tethered Satellite System During Retrieval.," *Proc. of the* 3^{rd} *VPI&SU/AIAA Symp. on Dynamics and Control of Large Flexible Spacecraft*, Blacksburg, VA, USA, Jun. 1981, pp. 453–469.

[15] V. J. Modi, G. Chang-Fu, A. K. Misra, and D. M. Xu, "On the Control of the Space Shuttle Based Tethered Systems," *Acta Astronautica*, Vol. 9, 1982, pp. 437–443.

[16] W. H. Clohessy and R. S. Wiltshire, "Terminal Guidance System for Satellite Rendezvous," *Journal of the Aerospace Sciences*, Vol. 27, Sept. 1960, pp. 653–658.

[17] G. W. Hill, "Researches in the Lunar Theory," *American Journal of Mathematics*, Vol. 1, No. 1, 1878, pp. 5–26.